Supplement of Atmos. Chem. Phys., 25, 4107–4129, 2025
https://doi.org/10.5194/acp-25-4107-2025-supplement

Atmospheric Chemistry and Physics
Open Access
EGU

Supplement of

Marine organic aerosol at Mace Head: effects from phytoplankton and source region variability

Emmanuel Chevassus et al.

Correspondence to: Jurgita Ovadnevaite (jurgita.ovadnevaite@universityofgalway.ie)

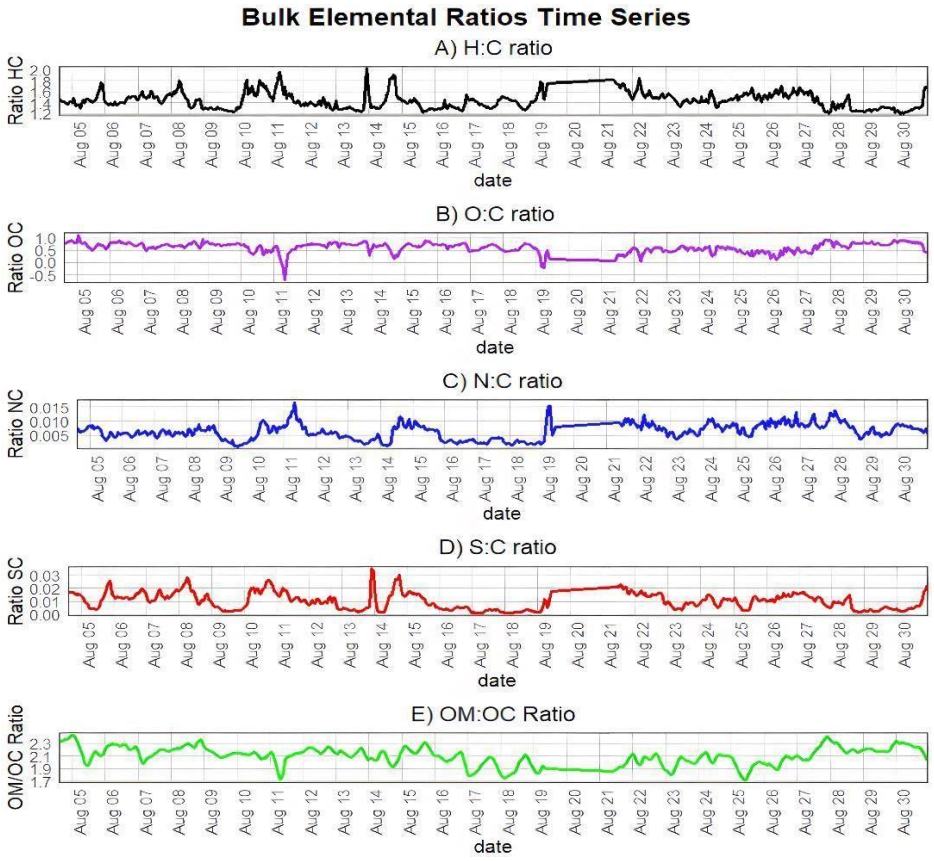

Figure S1. Elemental bulk ratios (H:C, O:C, N:C, S:C, and OM:OC) time series. The five panels show the hourly variations of A) Hydrogen-to-carbon (H:C) B) Oxygen-to-carbon (O:C) C) Nitrogen-to-carbon (N:C), D) Sulphur-to-carbon (S:C), and E) Organic matter-to-organic carbon (OM/OC) ratios, respectively.

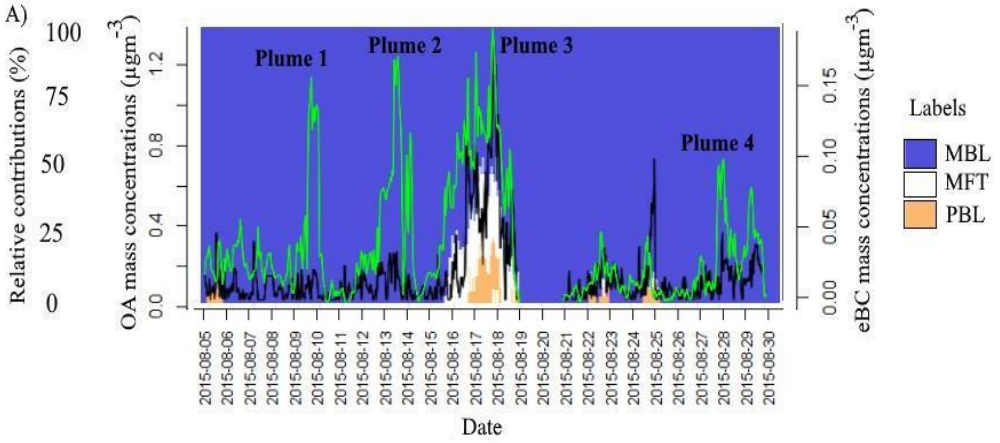

Figure S2. OA (green) and eBC (black) time series plotted alongside the fractional contribution of marine free troposphere (MFT), marine boundary layer (MBL) and planetary boundary layer (PBL). Many OA plumes happen in the MBL while a mixed episode 'Plume 3' had some PBL and MFT influence. Most of these OA plumes cover various regions of the West European Basin while 'Plume 4' specifically originates from Polar Air Masses.

Text S1. Positive Matrix Factorization (PMF) Model.

Organic mass spectra were processed with Positive Matrix Factorization (PMF) via the Toolkit Source Finder (SoFi) code in Igor Wavemetrics. Due to the low m/z values for large ions, only ions with m/z less than 130.07 were considered in this study. We performed the unconstrained PMF runs to examine a range of solutions with 1 to 11 factors. Reasonable results were obtained for factor numbers N=4 based on the resolved profiles (Figure S13). For N=4, MO-OOA was resolved according to oxidation state, O_3, O:C ratio, time series, mass spectral properties compared with previous studies. MSA-OA was resolved according to reconstructed MSA, SO_4 and mass spectral properties. PMOA was resolved according to reference mass spectra. Finally, Peat-OA was resolved according to eBC and mass spectral properties.

Compared to the N=4 solution, in the N=5 solution (Q/Qexp ratio=1.38), MO-OOA was further splatted into 2 factors (Figure S3) which appeared less meaningful compared to N=4 for which factors were more clearly identified. Furthermore, the Peat-OA factor was split into two factors, with the second factor being insignificant bearing no additional physical interpretation. Therefore, we reasoned that the N=4 solution was the most reasonable.

To further refine the solution and mitigate the rotational uncertainty, fpeak analysis was performed on the four-factor solution. The Q/Qexp ratio remained stable without any notable increases or decreases across an fpeak range of -1 to 1, as depicted in Figure S2. This suggests that the solution remains consistent across different fpeak values. Consequently, the solution with fpeak=0 was considered optimal. Additionally, the errors were found to be acceptable, with the maximum error below 5% and other errors also falling within acceptable ranges (Figure S1)

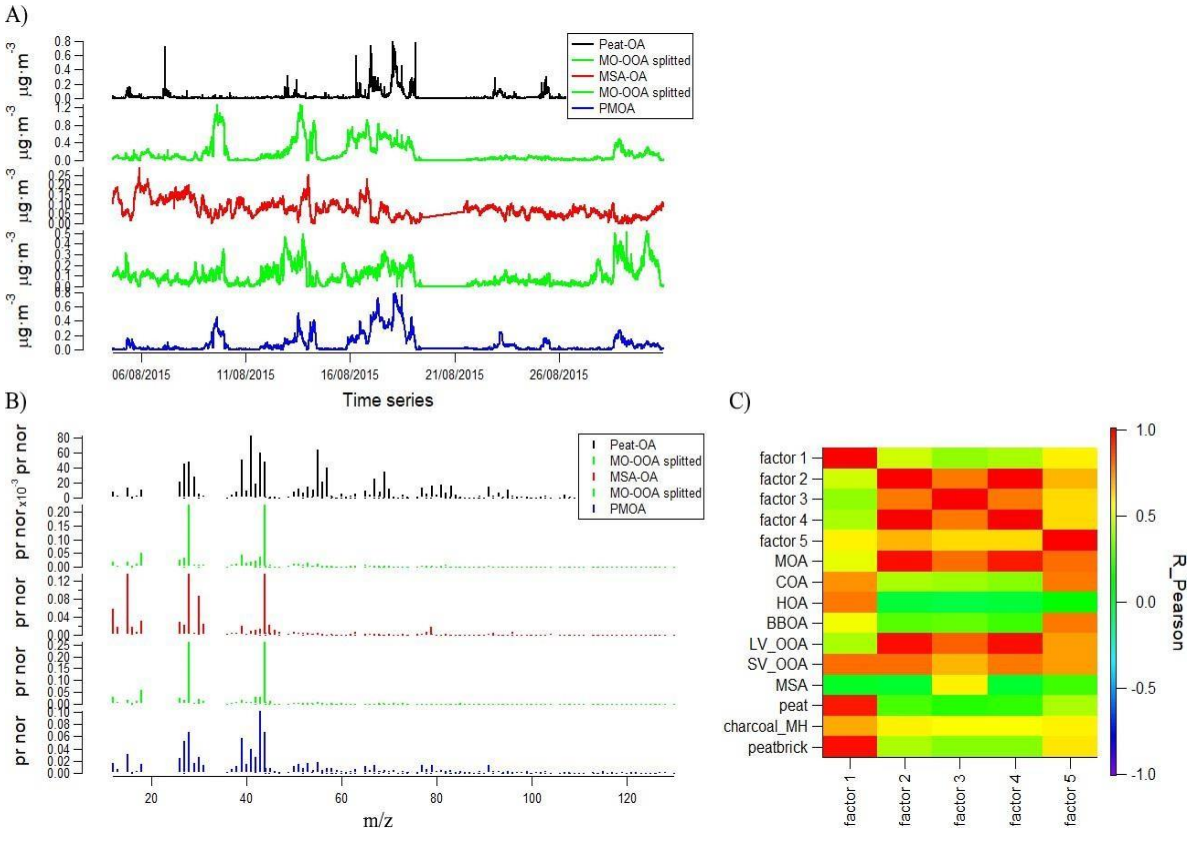

Figure S3: PMF metrics – 5 factors solution A) Times Series B) PMF Mass spectra C) Correlations with reference mass spectra.

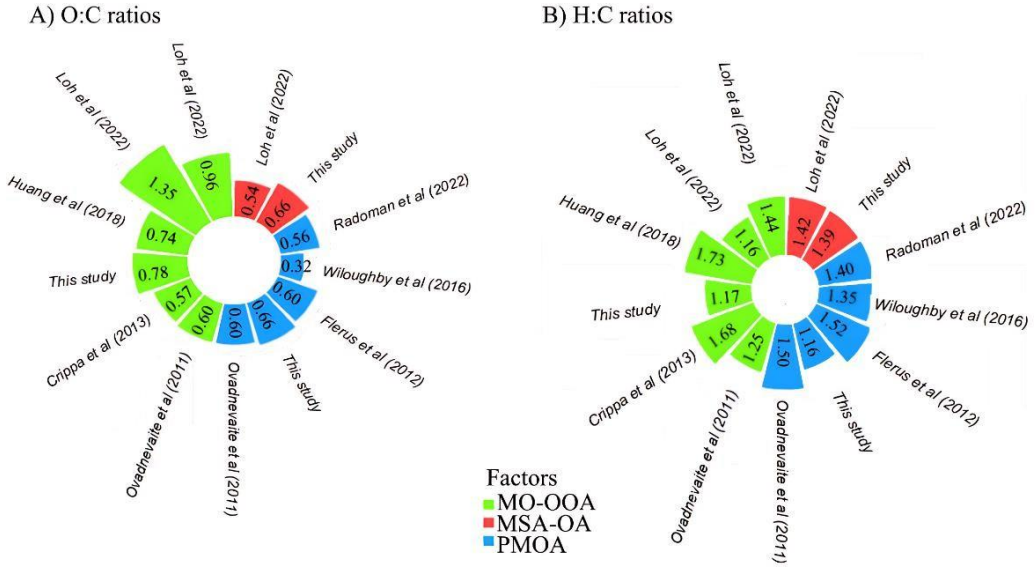

Figure S4. Circular bar plot, comparison between literature O:C and H:C ratios values for MO-OOA (green), MSA-OA (red) and PMOA (blue).

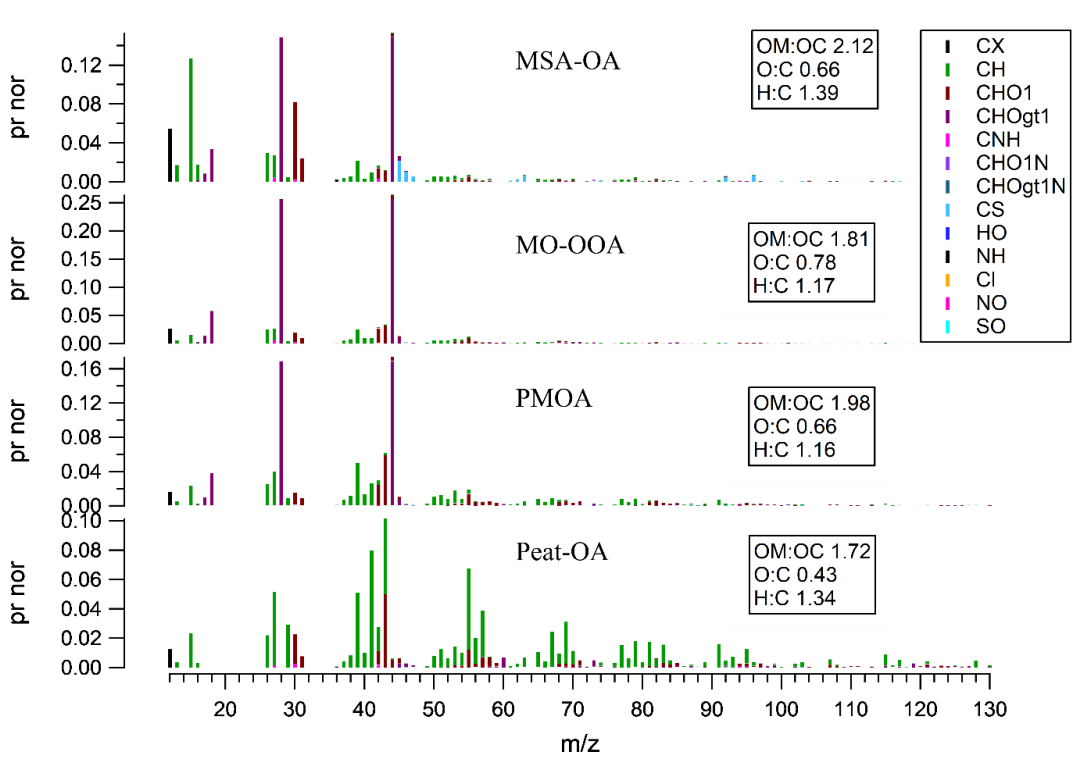

Figure S5. PMF factors HR families (Canagaratna - ambient method).

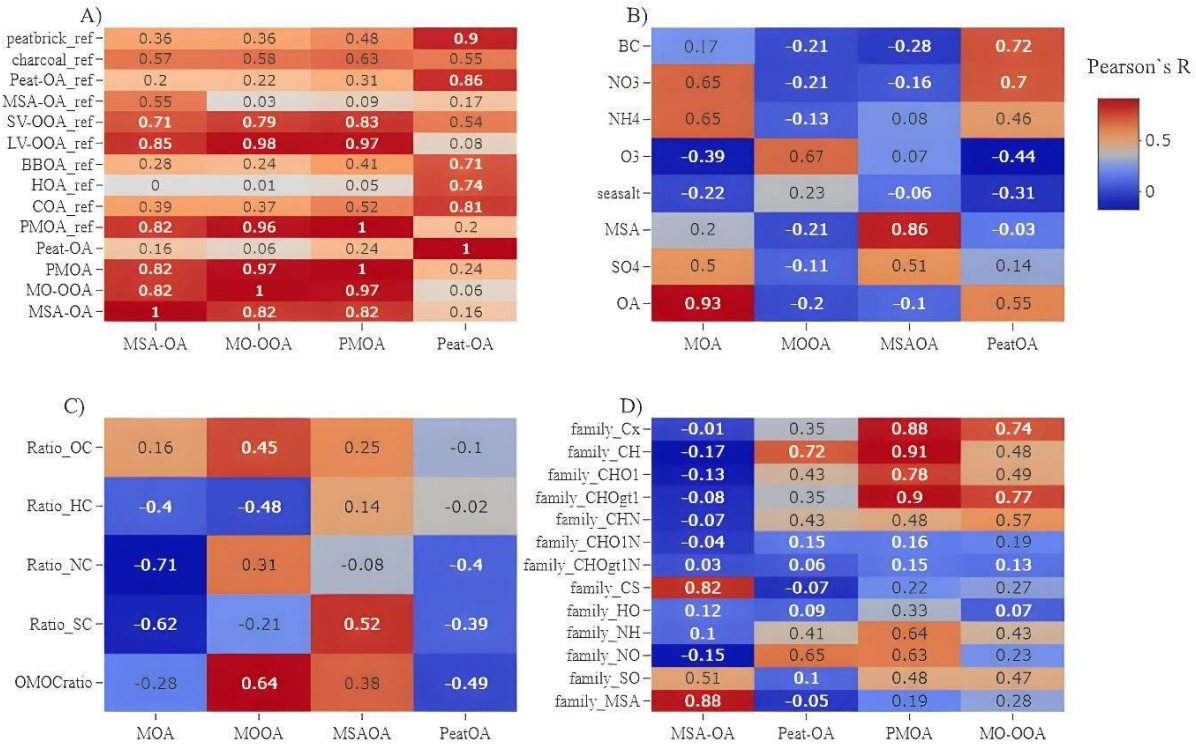

Figure S6. Pearson's correlation heatmaps of A) correlation between PMF mass spectra and reference mass spectra, B) correlation between PMF time series and external tracers time series, C) correlations between PMF time series and bulk elemental ratios time series, D) shows correlations between PMF times series and bulk OA families.

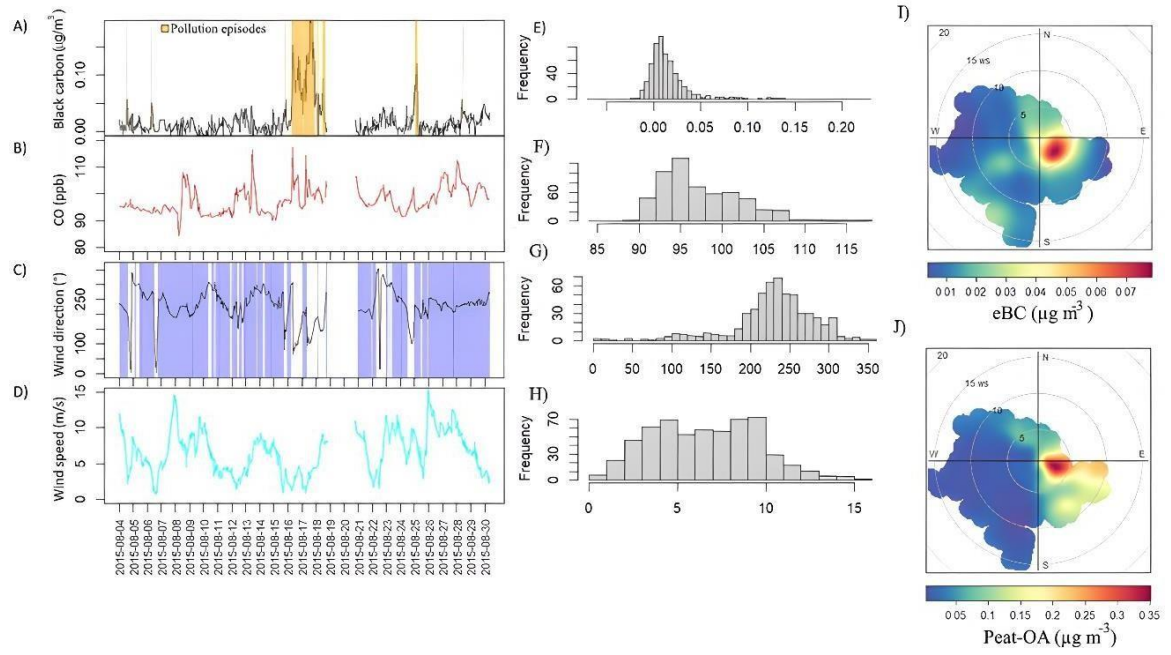

Figure S7. eBC mass concentrations time series, orange shaded areas represent eBC mass concentrations >50µg m^{-3} B) CO mixing ratio (ppb) C) Wind Direction, blue shaded areas represent marine sector (190-300°) D) Wind speed (m/s) I) eBC pollution wind rose J) Peat-OA pollution wind rose. Histograms associated to each time series are represented in the middle panel.

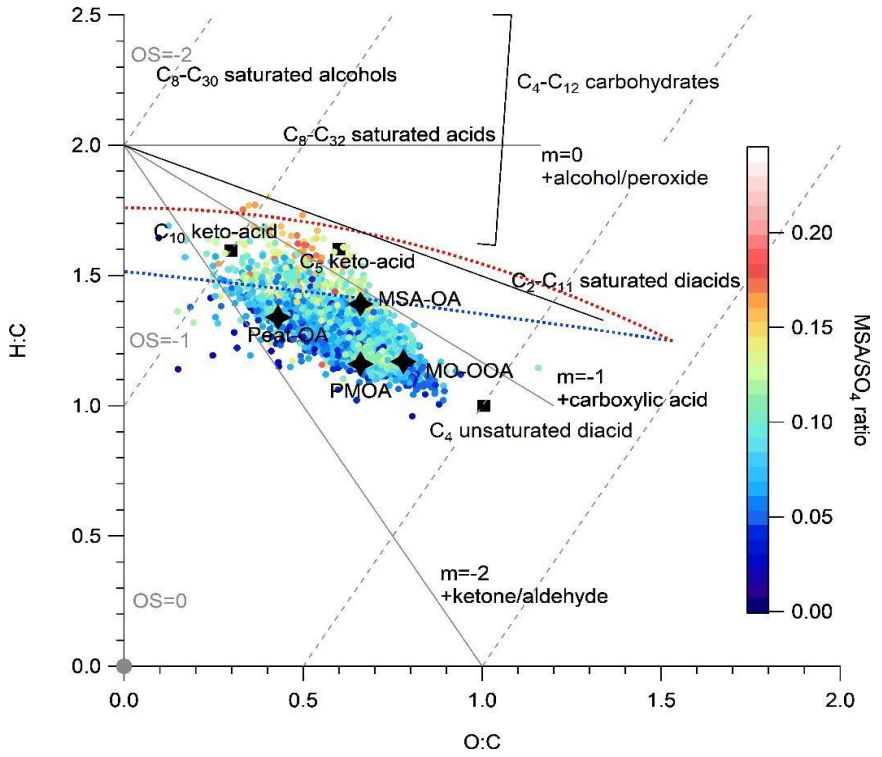

Figure S8. Relationship between the ToF-AMS estimated oxygen-to-carbon (O/C) and hydrogen-to-carbon (H/C) ratios of organic species (Canagaratna et al., 2015) coloured by the MSA-to-sulphate ratio. Grey lines represent functional groups (Ng et al., 2011) while dashed line represent the average carbon oxidation state (OSc ≈ 2 × O : C − H : C) superimposed on the Van Krevelen diagram (Kroll et al., 2011). Elemental composition of C_8–C_{30} saturated alcohols, C_8–C_{32} saturated acids, C_2 –C_{11} saturated diacids, C_4 unsaturated diacid (maleic and fumaric acid), C_4 –C_{12} carbohydrates and derivatives (e.g., trehalose, erythritol, arabitol, mannitol, sucrose, galactose, glucose, and fructose), and C_5 and C_{10} ketoacids (levulinic and pinonic acid, respectively) are shown for reference (Willis et al., 2017).

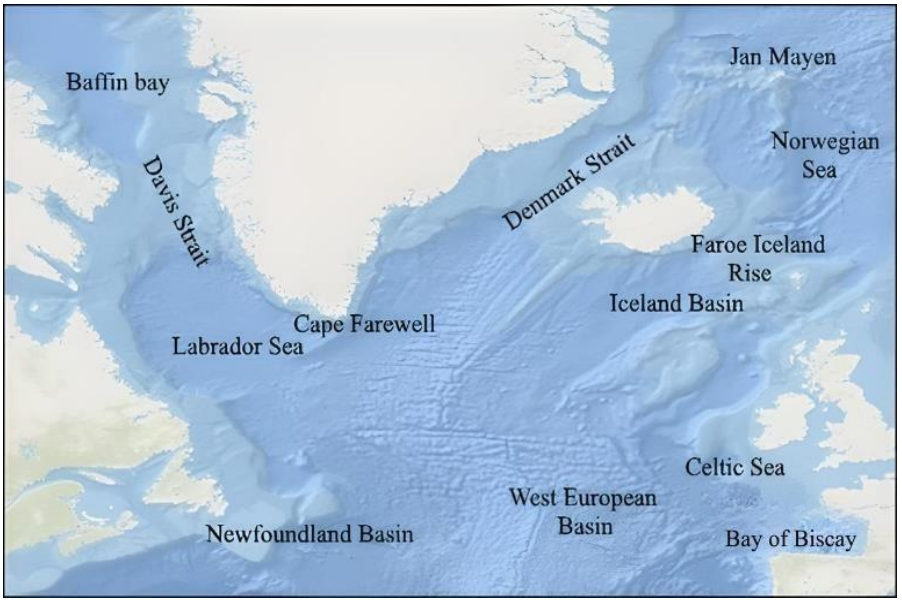

Figure S9. Descriptive toponymy of Ocean areas of interest and landmarks. Background Map from © OpenStreetMap contributors 2023. Distributed under the Open Data Commons Open Database License (ODbL) v1.0.

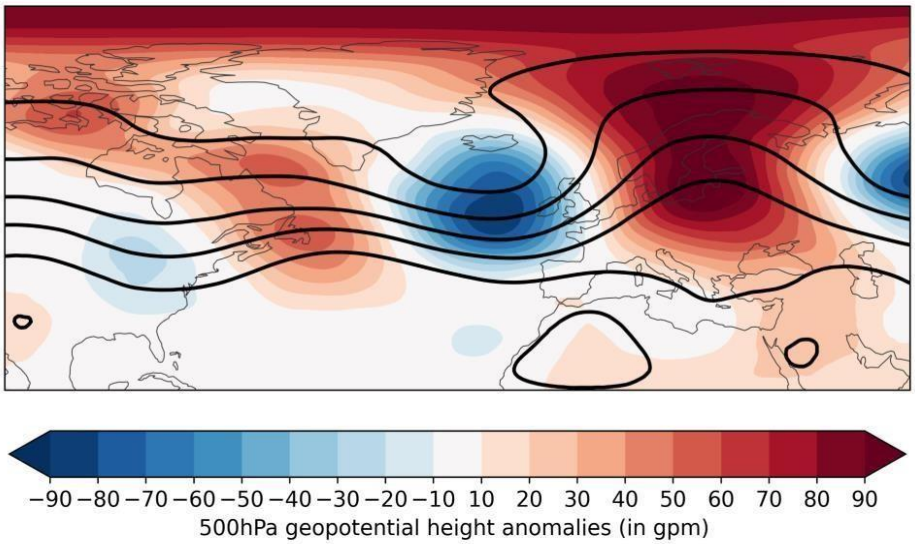

Figure S10 - 500hPa geopotential height anomalies (in gpm) highlighting anticyclonic blocking (in red) calculated from ERA5 (Hauser et al., 2024; Hersbach et al., 2020).

References

Canagaratna, M. R., Jimenez, J. L., Kroll, J. H., Chen, Q., Kessler, S. H., Massoli, P., Hildebrandt Ruiz, L., Fortner, E., Williams, L. R., Wilson, K. R., Surratt, J. D., Donahue, N. M., Jayne, J. T., and Worsnop, D. R.: Elemental ratio measurements of organic compounds using aerosol mass spectrometry: characterization, improved calibration, and implications, Atmos. Chem. Phys., 15, 253–272, https://doi.org/10.5194/acp-15-253-2015, 2015.

Hauser, S., Teubler, F., Riemer, M., Knippertz, P., and Grams, C. M.: Life cycle dynamics of Greenland blocking from a potential vorticity perspective, Weather Clim. Dynam., 5, 633–658, https://doi.org/10.5194/wcd-5-633-2024, 2024.

Hersbach, H., Bell, B., Berrisford, P., Hirahara, S., Horányi, A., Muñoz-Sabater, J., Nicolas, J., Peubey, C., Radu, R., Schepers, D., Simmons, A., Soci, C., Abdalla, S., Abellan, X., Balsamo, G., Bechtold, P., Biavati, G., Bidlot, J., Bonavita, M., Chiara, G., Dahlgren, P., Dee, D., Diamantakis, M., Dragani, R., Flemming, J., Forbes, R., Fuentes, M., Geer, A., Haimberger, L., Healy, S., Hogan, R. J., Hólm, E., Janisková, M., Keeley, S., Laloyaux, P., Lopez, P., Lupu, C., Radnoti, G., Rosnay, P., Rozum, I., Vamborg, F., Villaume, S., and Thépaut, J.: The ERA5 global reanalysis, Q.J.R. Meteorol. Soc., 146, 1999–2049, https://doi.org/10.1002/qj.3803, 2020.

Kroll, J. H., Donahue, N. M., Jimenez, J. L., Kessler, S. H., Canagaratna, M. R., Wilson, K. R., Altieri, K. E., Mazzoleni, L. R., Wozniak, A. S., Bluhm, H., Mysak, E. R., Smith, J. D., Kolb, C. E., and Worsnop, D. R.: Carbon oxidation state as a metric for describing the chemistry of atmospheric organic aerosol, Nature Chem, 3, 133–139, https://doi.org/10.1038/nchem.948, 2011.

Ng, N. L., Canagaratna, M. R., Jimenez, J. L., Chhabra, P. S., Seinfeld, J. H., and Worsnop, D. R.: Changes in organic aerosol composition with aging inferred from aerosol mass spectra, Atmos. Chem. Phys., 11, 6465–6474, https://doi.org/10.5194/acp-11-6465-2011, 2011.

Willis, M. D., Köllner, F., Burkart, J., Bozem, H., Thomas, J. L., Schneider, J., Aliabadi, A. A., Hoor, P. M., Schulz, H., Herber, A. B., Leaitch, W. R., and Abbatt, J. P. D.: Evidence for marine biogenic influence on summertime Arctic aerosol, Geophys. Res. Lett., 44, 6460–6470, https://doi.org/10.1002/2017GL073359, 2017.